

Electrochemical Behavior of NiAl and Ni₃Al Intermetallic Coatings in 1.0 M NaOH Solution

J. Porcayo-Calderon^{1,2,*}, O. Sotelo-Mazon¹, A. Luna-Ramirez³, E. Porcayo-Palafox¹,
V.M. Salinas-Bravo³, L. Martinez-Gomez^{2,4}

¹Universidad Autonoma del Estado de Morelos, CIICAp, Av. Universidad 1001, 62209 Cuernavaca, Morelos, Mexico

²Universidad Nacional Autonoma de Mexico, Instituto de Ciencias Fisicas, Av. Universidad s/n, 62210 Cuernavaca, Morelos, Mexico

³Instituto de Investigaciones Electricas, Reforma 113, 62490 Cuernavaca, Morelos, Mexico

⁴Corrosión y Protección (CyP), Buffon 46, 11590 Mexico City, DF, Mexico

*E-mail: jporcayoc@gmail.com

Received: 20 March 2015 / Accepted: 26 May 2015 / Published: 24 June 2015

Three different grain sizes were used to deposit NiAl and Ni₃Al intermetallic coatings on 304 type SS by thermal spraying powder and HVOF (High Velocity Oxygen Fuel) processes. Coatings were characterized by scanning electron microscopy and their characteristics are described as a function of particle size and coating process applied. The corrosion resistance of coatings was evaluated through open circuit potential, potentiodynamic polarization and linear polarization resistance tests in a 1.0 M NaOH solution at room temperature (25 °C). It was observed that the spray process and the particle size have an effect on the electrochemical behavior of coatings tested. Different coatings showed no significant variations in current densities, but were one order of magnitude greater than those of the base alloy; corrosion potentials of coatings were more negative than those of its base alloy regardless of particle size and have similar values.

Keywords: Intermetallics coatings, nickel aluminides, corrosion, thermal spray, HVOF

1. INTRODUCTION

Some advantageous properties, at high temperatures (> 650 °C), of the Ni-based intermetallic compounds are a high resistance to oxidation and carburization, high fatigue resistance, excellent wear resistance, good tensile and compressive yield strength. Some of its possible industrial applications can be, heat treating trays, die blocks, centrifugally cast tubes, single crystal turbine blades, corrosion resistance tool bits, automotive turbochargers, and pistons and valves, among other applications [1].

The corrosion resistance of intermetallic alloys at room temperature is one of the main requirements which determine the application of a high temperature alloy. At room temperature, the intermetallic compounds can be damaged by corrosion when exposed to harsh environments. Limited literature data exists on corrosion behavior of Ni-Al based intermetallic [2, 3] and Ni-Al based intermetallic used as coatings applied by thermal spraying process in aqueous solution at room temperature [4].

The thermal spraying is a viable process for the deposition of a large amount of materials to form a coating. The thermal spraying process has been used for the deposition of intermetallic compounds, where the metal powders were obtained by different processes such as inert gas atomization, inert gas atomization and subsequent milling, mechanical alloying and high temperature synthesis [5-13]. However, few studies have been reported where the intermetallic powder is obtained milling the ingot [14]. Intermetallic coatings have been applied by different processes as HVOF [5-6, 8-11, 15-24], electro-welding [26] and plasma spraying [8, 12-14, 27].

The main advantage of utilizing a process of high kinetic energy for coating is that coatings are of higher density, greater thickness, a smoother surface, low oxides and less effect on the environment (reduced oxidation and decarburization and lower key elements loss by vaporization) [23].

This paper reports the performance of NiAl and Ni₃Al coatings deposited by HVOF and flame spraying processes. Coatings were characterized microstructurally and the corrosion resistance was evaluated in 1.0 M NaOH at 25 °C.

2. EXPERIMENTAL

2.1. Material and sample preparation

Intermetallic alloys were obtained by melting high purity elements (> 99.95%) in the stoichiometric ratios for Ni₃Al and NiAl compounds. The melt was performed in an induction furnace under inert atmosphere, and after that the melt was cast in molds. The intermetallic alloys were ground in a hammer mill to a particle size around 3 mm in diameter, and after that pulverized in a ball mill. After that, metallic powders were classified in a vibrating mesh.

Table 1. Chemical composition of the intermetallic powder alloys.

Powder alloy	Concentration (weight %)	
	Al	Ni
Ni ₃ Al	12.86	Balance
NiAl	27.62	Balance

Chemical composition of the powder alloys as determined by atomic absorption spectroscopy are reported in Table 1. Powder alloys were classified in three different particles sizes. Namely, coarse particle size were the powder alloys with particle size between 56-84 μm , medium particle size the powder alloys between 56-41 μm , and the fine particle size the powder alloys with particle size less than 41 μm .

2.2. Thermal spray processes

Different coatings were applied onto 304 stainless steel bars. Thermal spray processes used were the thermal spray of metallic powders by oxy-acetylene flame, and HVOF process (High Velocity Oxygen-Fuel). The equipment used for the coatings application were a Sulzer-Metco gun 5PII model and a Sulzer-Metco model DJ2700, respectively. Before the coating application, substrates were superficially prepared by grit blast according to the NACE standard 1/SSPC-SP No. 5, and degreased with acetone prior to the application of coatings.

2.3. Electrochemical test

Coatings and alloys were evaluated by potentiodynamic polarization, open circuit potential (E_{corr}) and linear polarization resistance (LPR) measurements. Electrochemical cell consisted of a three-electrode arrangement, where the reference electrode was a saturated calomel electrode (SCE), a platinum wire as counter electrode (CE), and the working electrode were the coatings and intermetallic alloys. Coatings and alloys were evaluated in a 1.0 M NaOH solution ($\text{pH} = 13.54$) at room temperature without aeration during 30 days. Potentiodynamic polarization measurements were from -300 mV to 2000 mV regarding the corrosion potential (E_{corr}) at a scan rate of 60 mV/min. LPR measurements were performed at a scanning rate of 10 mV/min in ± 20 mV span.

3. RESULTS AND DISCUSSION

3.1. X-ray diffraction of powders alloys

XRD diffraction patterns for the intermetallic powder alloys used are shown in Figure 1. In both cases, the identified peaks correspond to the NiAl and Ni₃Al intermetallic compounds as it has been reported by other authors [2]. It is said that the width of the peaks is related to the size reduction of the metallic powder, and with the presence of stresses in the grain due to plastic deformation during the milling [28]. In general, NiAl alloy was more brittle than the Ni₃Al alloy, and therefore easier to grind, and thus their peaks are not as wide as those observed in the Ni₃Al powders.

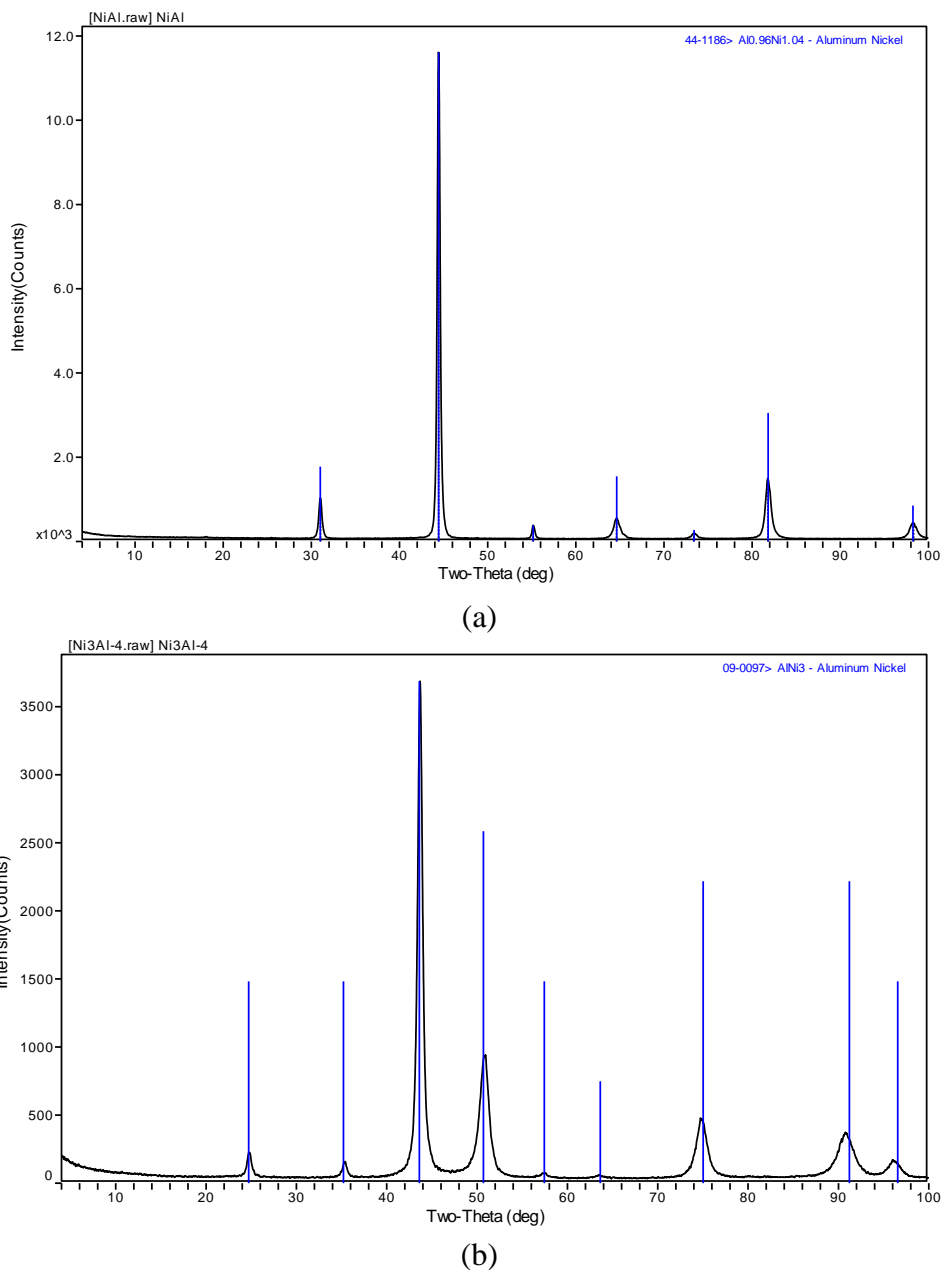


Figure 1. XRD patterns of (a) NiAl and (b) Ni₃Al powder alloy.

3.2. Coating surface appearance

Figure 2 shows the appearance of Ni₃Al and NiAl particles deposited by the process of oxy-acetylene flame. In the case of medium and fine particle size (Fig. 2b, 2c, 2e and 2f), the presence of splashes and fractionating of particles at impact. In the case of coarse particle size (Fig. 2a, 2d) it is observed that even when the deformation of the particles is achieved it can be seen some particles that are not completely deformed. This may be due that even though the oxy-acetylene flame temperature is high enough (3000 °C) to completely melt the particles, the residence time of the particles in the region of the flame is not enough to melt them or the kinetic energy at impact is not high enough to achieve deformation.

Figure 3 shows the appearance of Ni₃Al and NiAl particles deposited by the HVOF process. The HVOF process (Fig. 3a) shows that the operating parameters were not sufficient to completely melt the coarse grain particles. This is justified by the fact that in this process the temperature of the flame is much lower (~2500 °C) and because the residence time in the supersonic flame is very small so particles are not completely melted or when impacting the substrate do not achieve full deformation [29]. In the case of the medium grain size particles (Fig. 3b, 3e) it was observed particles completely melted and deformed as well as particles that apparently are not completely deformed upon impact but which are incorporated appropriately in the coating. Appearance with fine grain particles (Fig 3c, 3f), shows that particles are completely molten and deformed upon impact, showing that dense coatings were obtained.

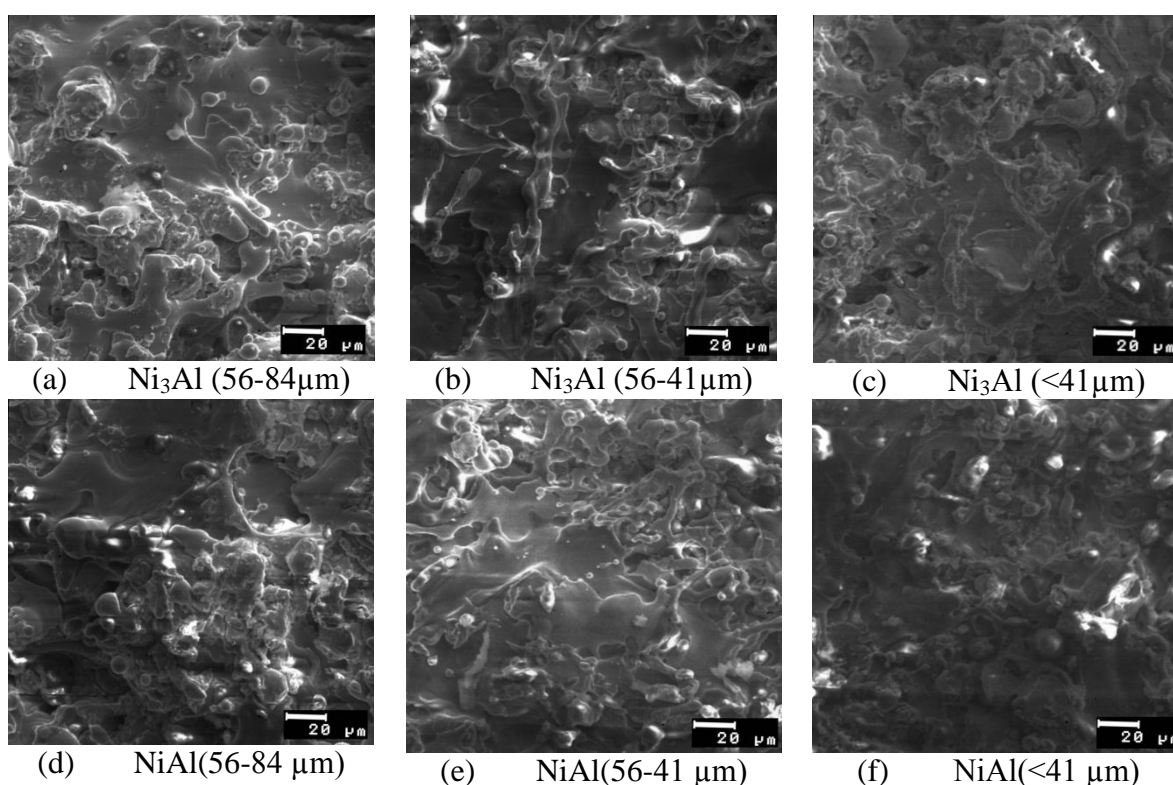
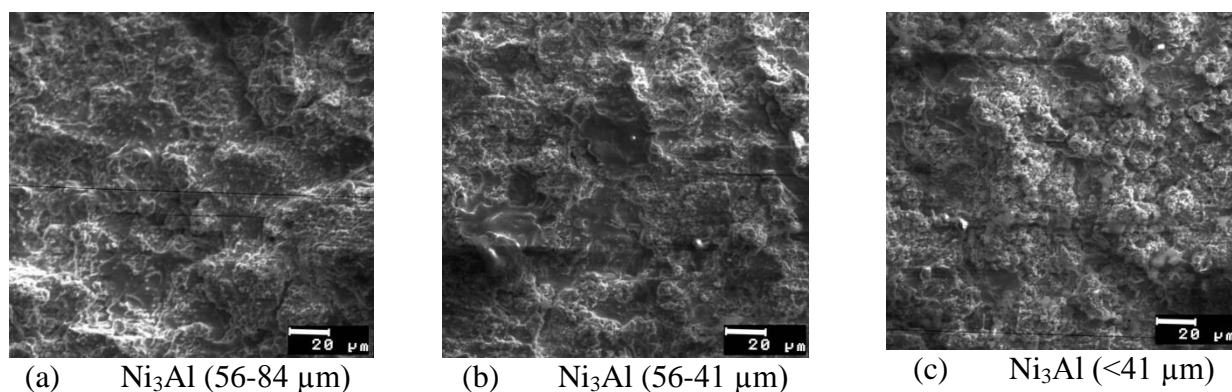


Figure 2. Surface images of Ni₃Al and NiAl coatings deposited by the powder flame spray process



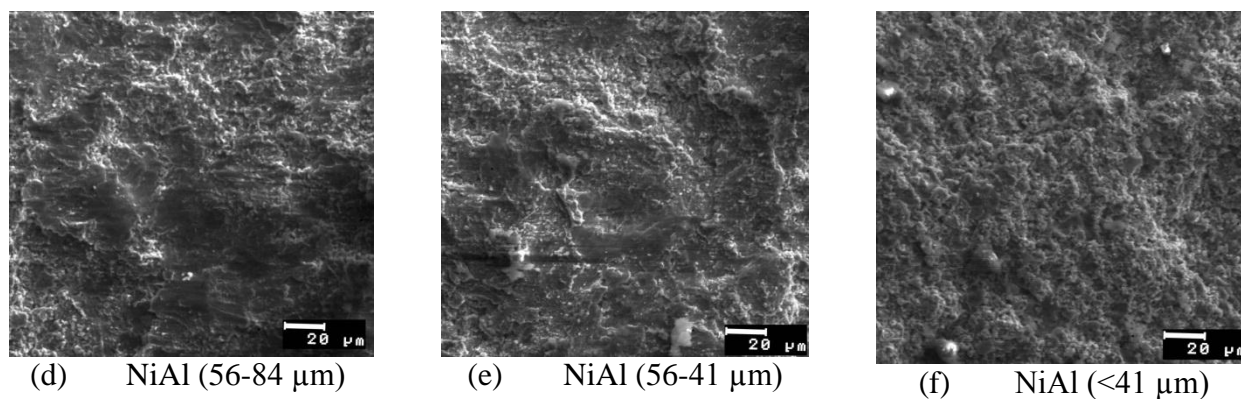


Figure 3. Surface images of Ni_3Al and NiAl coatings deposited by coatings HVOF process.

Foundation of HVOF technology focuses on high kinetic energy of the particles. This energy at impact transforms into heat achieving melting, deformation and compact stack with a high density in such coatings [29].

3.3. Cross section of coatings

Figures 4 and 5 show the cross section area of coatings applied by flame spray and HVOF processes. Coatings applied by flame spray process, are heterogeneous. They have a laminar structure parallel to the substrate, porosity, partially molten particles, partially fractured particles and presence of trapped oxides [29]. These features are seen in all cases regardless of the particle size of the powder material. An important observation is the presence of oxide phases located between the layers of the coating. These phases appear dark and grey in Figures 4 and 5. They increase by decreasing particle size. Aluminum content is higher in dark phases and nickel content is lower in grey and clear phases [27]. The three types of particle size used have acceptable features. It would depend on the analysis of porosity, oxide content and perhaps micro hardness to define the most appropriate particle size for such deposition process.

Regarding the HVOF process, Figure 5 shows the main features. It was observed that coatings showed greater density than flame spray coatings. In the case of coatings deposited from powders with coarse particle is observed that not all the particles reach an energy state to allow them full deformation upon impact. In addition, its cohesion with other particles is low because during metallographic preparation of specimens some layers were separated (Fig. 5a). Coatings obtained with medium and fine particle sizes show better properties than similar coatings applied by the process of projection of powders by flame; an important difference is the absence of the dark grey and light phases observed in the flame deposition process.

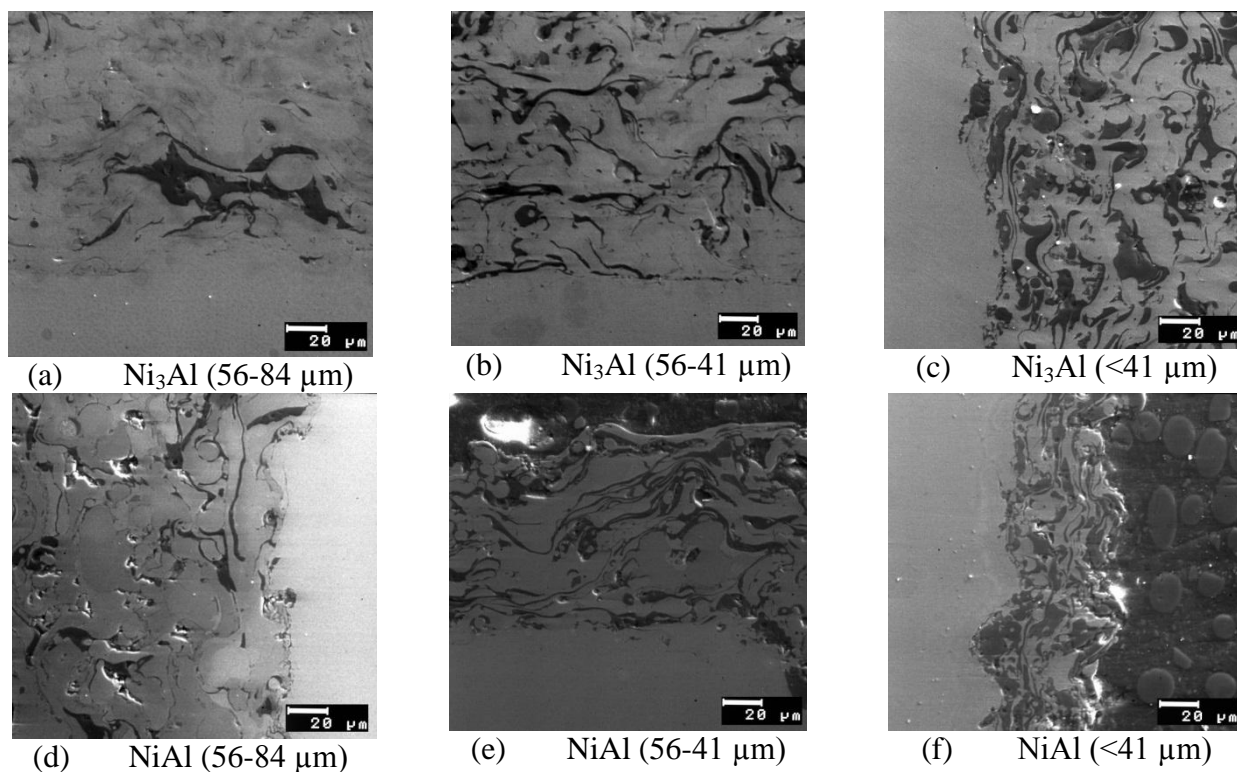


Figure 4. Cross section area of Ni_3Al and NiAl coatings deposited by powder flame spray process.

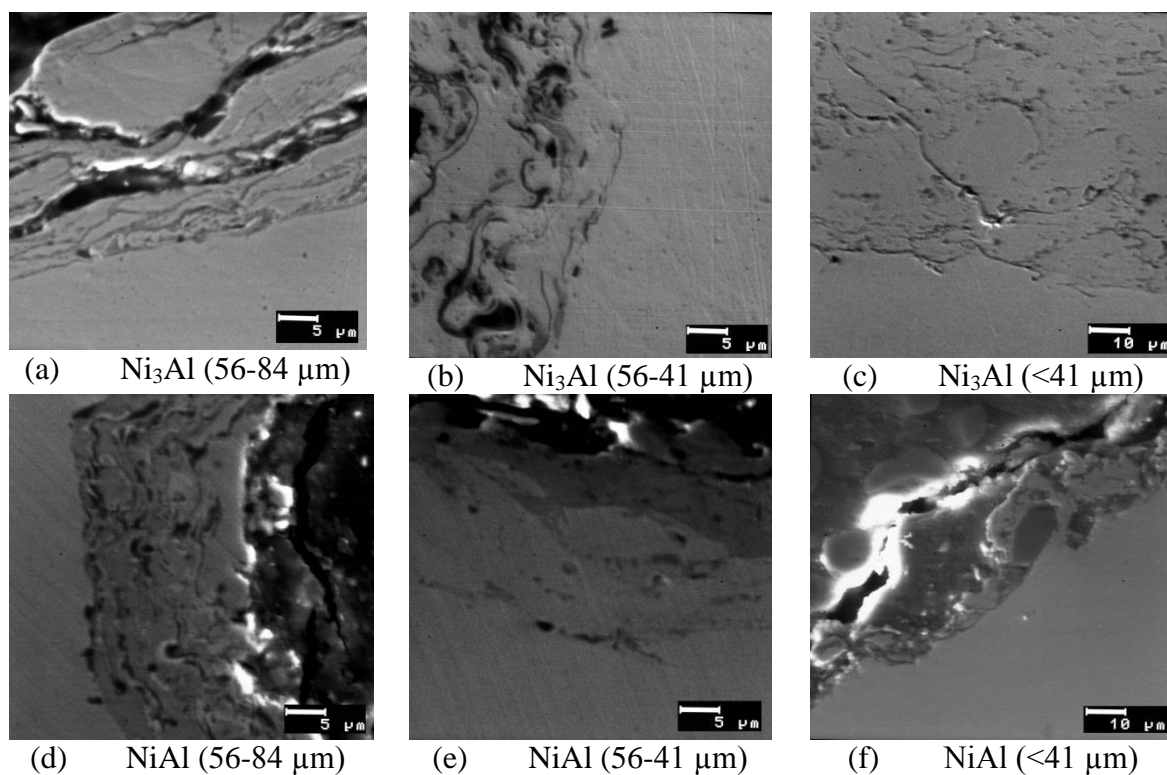


Figure 5. Cross section area of Ni_3Al and NiAl coatings deposited by HVOF.

Coatings deposited by the powder flame spray process showed significant porosity, presence of oxides and a greater fraction of unmelted particles. However, coatings produced by the HVOF process showed lower porosity, fewer oxides and little fraction of unmelted particles. This latter feature diminishes as the velocity of the particle projection increases. This is explained because reducing the particles flight duration they have less time for oxidation reactions. This clarifies why coatings deposited by HVOF process have a reduced amount of oxides [30-32].

3.4. Electrochemical measurements

3.4.1. Polarization tests

Figure 6 shows polarization curves of 304 stainless steel and Ni₃Al and NiAl intermetallic alloys evaluated in 1.0 M NaOH at 25 °C. 304 stainless steel has a tendency to increase its current density depending on the applied potential, and subsequently decreased to reach a passivity zone around -70 mV. Its corrosion potential was -410 mV and i_{corr} value of 0.0013 mA/cm². Ni₃Al intermetallic alloy practically had the same corrosion potential of stainless steel (-406 mV), and around -100 to 300 mV an apparent passive zone is observed. The corrosion current density was 0.0001 mA/cm², an order of magnitude less than that of stainless steel. The corrosion potential of Ni₃Al obtained in this work is similar to that obtained by other investigators [2].

NiAl intermetallic alloy showed a corrosion potential more cathodic (-682 mV). It was observed an increase in current density by increasing the potential up to -230 mV; from this value it tends to decrease until it reaches the start a passive zone at approximately -250 mV. The corrosion current density (0.0019 mA/cm²) was similar to that measured in 304 stainless steel. Table 2 shows a summary of the electrochemical parameters obtained from potentiodynamic polarization curves.

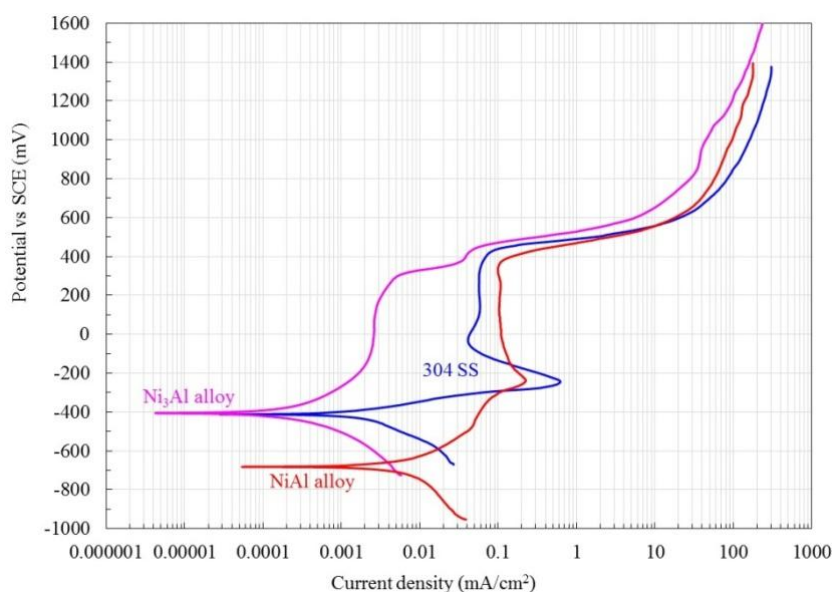


Figure 6. Polarization curves of Ni-Al base alloys and 304 S.S in 1.0 M NaOH at 25 °C.

Table 2. Electrochemical parameters for NiAl and Ni₃Al base alloys and 304 SS in 1.0 M NaOH at 25 °C.

Material	E_{corr} (mV)	i_{corr} (mA/cm ²)	β_a	β_c
304 SS	-410	0.0013	76.9	156.5
Ni ₃ Al	-406	0.0001	112.5	96.7
NiAl	-682	0.0019	70.9	69.5

Figure 7 shows the behavior of Ni₃Al coatings deposited by flame sprayed process (5PII) evaluated in 1.0 M NaOH at 25 °C. It is observed that powder grain size has influence on the coating corrosion potential. Coatings with the smaller particle size had the noblest corrosion potential. This behavior is associated with the oxidation phenomenon experienced during spraying. Smaller particles have a greater tendency to oxidize due to reaching higher temperatures [33]. Additionally, the coating structure has many oxides trapped. Regarding corrosion current density, Ni₃Al intermetallic powders have higher values than the intermetallic base alloy, i_{corr} values determined for Ni₃Al coatings are 0.005, 0.0012 and 0.0017 mA/cm² for the coarse, medium and small grain size respectively. This implies that smaller particle size corresponds to lower corrosion rate. All coatings showed a clear passivation zone. Coarse grain size coating passivation starts from -700 mV, medium grain size coating starts from approximately -400 mV, and fine grain coating starts from -620 mV.

Figure 8 shows polarization curves of NiAl coatings deposited by the flame sprayed process evaluated in 1.0 M NaOH at 25 °C. Current density values were 0.022, 0.0022 and 0.0003 mA/cm² for coarse, medium and fine grain size respectively. A difference of an order of magnitude between each grain size indicates again that smaller particle size results in lower corrosion rates. The fine grain size coating does not show a defined passive zone, the passivation zone in medium grain size coating starts from the -400 mV and at -600 mV in the coarse grain size coating. In all three coatings, the passivation zone ends at about -300 mV, initiating a transpassive zone. Table 3 shows a summary of the electrochemical parameters obtained from potentiodynamic polarization curves.

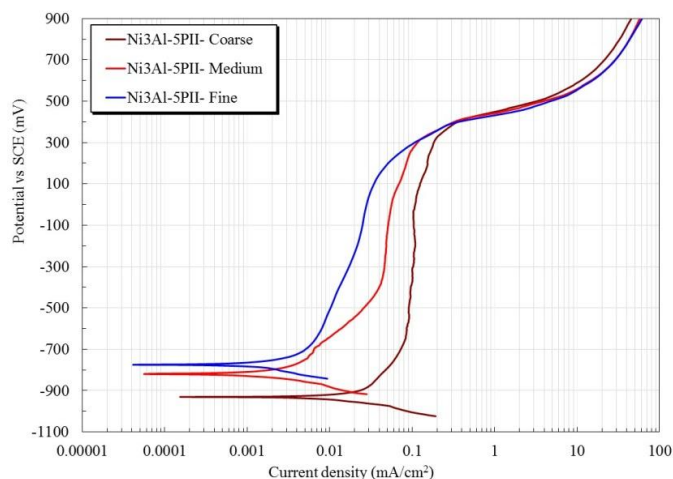


Figure 7. Polarization curves of Ni₃Al coatings deposited by powder flame spray process in 1.0 M NaOH at 25 °C.

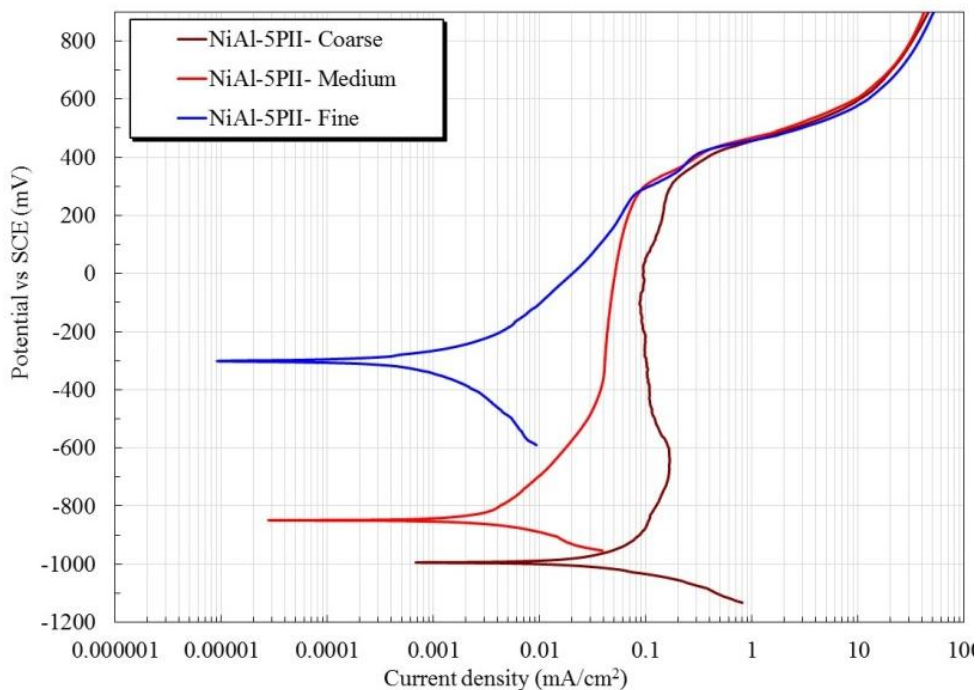


Figure 8. Polarization curves of NiAl coatings deposited by powder flame spray process in 1.0 M NaOH at 25 °C.

Table 3. Electrochemical parameters of Ni₃Al and NiAl coatings deposited by powder flame process (5PII) in 1.0 M NaOH at room temperature.

Coatings	Coarse particle size				Medium particle size				Fine particle size			
	E_{corr} (mV)	i_{corr} (mA/cm ²)	β_a	β_c	E_{corr} (mV)	i_{corr} (mA/cm ²)	β_a	β_c	E_{corr} (mV)	i_{corr} (mA/cm ²)	β_a	β_c
Ni ₃ Al	-930	0.005	43.8	44.5	-820	0.0012	89.6	61.2	-775	0.0017	140.7	88.8
NiAl	-993	0.022	107	57.1	-850	0.0022	196.9	63.3	-300	0.0003	70.5	79.2

In Figures 9 and 10 the performance of the coatings deposited by HVOF process is shown. In the case of Ni₃Al, unlike the coarse grained coating, medium and small size particle coatings showed almost the same electrochemical behavior, i.e. similar corrosion potential and corrosion densities. Corrosion potentials of all coatings were more negative than that of the base alloy (-406 mV). Regarding corrosion current density, all coatings have greater values than the base alloy (0.0001 mA/cm²) alloy, being of 0.0021, 0.022 and 0.013 mA/cm² for coatings of coarse, medium and fine grain size respectively. Similarly NiAl coatings showed very similar behavior regarding corrosion potential and current density. Corrosion potential was more cathodic than base alloy [34, 35]. Table 4 shows a summary of the electrochemical parameters obtained from potentiodynamic polarization curves.

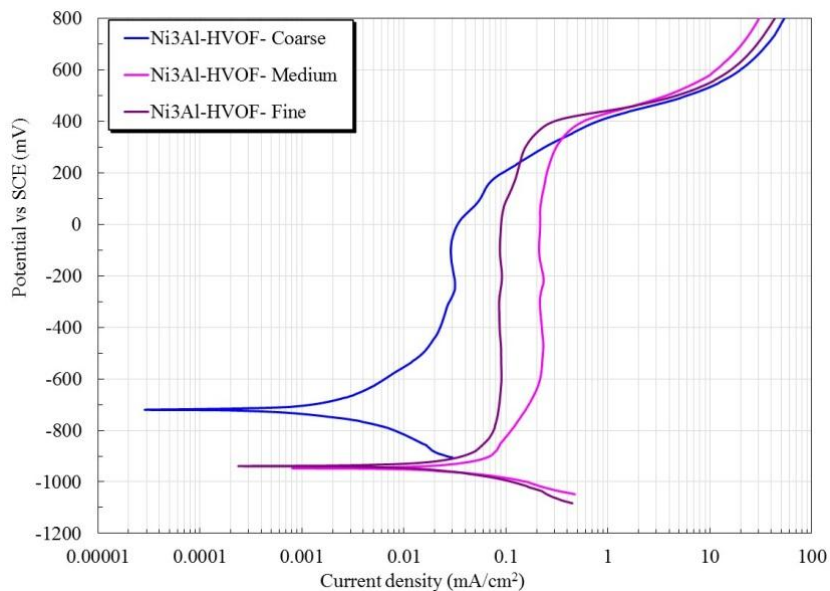


Figure 9. Polarization curves of Ni₃Al coatings deposited by the HVOF process in 1.0 M NaOH at 25 °C.

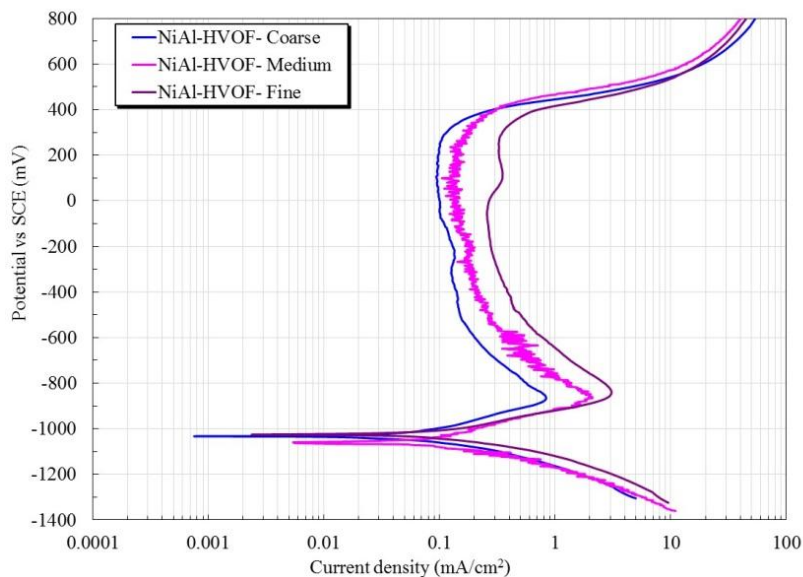


Figure 10. Polarization curves of NiAl coatings deposited by the HVOF process in 1.0 M NaOH at 25 °C.

Table 4. Electrochemical parameters of Ni₃Al and NiAl coatings deposited by the HVOF process in 1.0 M NaOH at room temperature.

Coatings	Coarse particle size				Medium particle size				Fine particle size			
	E_{corr} (mV)	i_{corr} (mA/cm ²)	β_a	β_c	E_{corr} (mV)	i_{corr} (mA/cm ²)	β_a	β_c	E_{corr} (mV)	i_{corr} (mA/cm ²)	β_a	β_c
Ni ₃ Al	-720	0.0021	245.5	140.3	-940	0.022	86.9	57.4	-938	0.013	85.6	59
NiAl	-1032	0.031	76.8	57.9	-1061	0.074	104.7	88	-1025	0.095	104.5	84.9

3.4.2 Open circuit potential

Figures 11 and 12 show the measured open circuit potential for 30 days of base alloys and coatings evaluated in 1.0 M NaOH at 25 °C. It is observed that in case of 304 stainless steel, the potential tends to increase slowly from -350 mV to -300 mV and remain constant throughout the test period. In case of the intermetallic Ni₃Al alloy its potential remained oscillating all the time. Potential of NiAl intermetallic alloy tend to increase drastically during the first 4 days and then remain constant with values close to that of stainless steel.

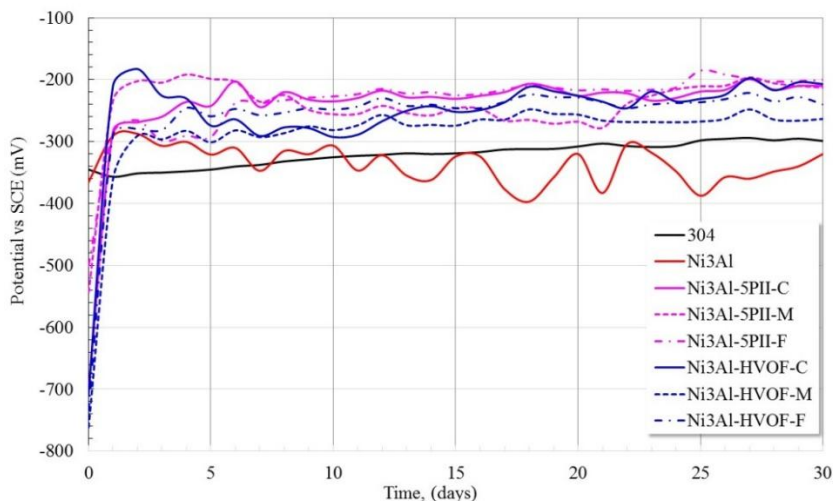


Figure 11. E_{corr} values measured at different testing time for Ni₃Al coatings and alloys in 1.0 M NaOH solution at 25 °C.

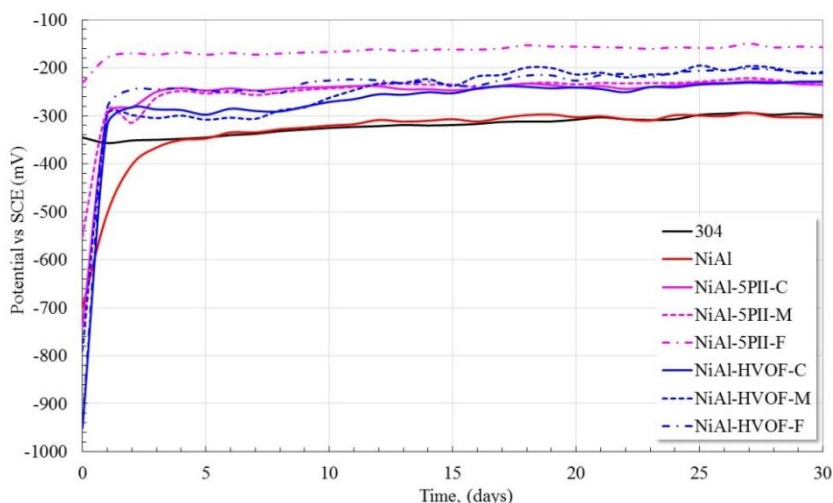


Figure 12. E_{corr} values measured at different testing time for NiAl coatings and alloys in 1.0 M NaOH solution at 25 °C.

All Ni₃Al coatings (irrespective of deposition process) tend to dramatically increase the corrosion potential within 24 hours of immersion to remain nearly constant but later reaching more positive values than Ni₃Al intermetallic alloy (Figure 11). It can be established that the increase in E_{corr} values in the first hours may be associated with many factors such as formation and thickening of the passive film [2], adsorption of species, dissolution of oxides and changes in the concentration of metal ions and oxygen. These factors favor the progress of diffusion layers that alter the surface activity as the electrolyte penetrates the porosity of the coating [36]. After 24 hours immersion, all intermetallic alloys showed a slight increase in corrosion potential reaching higher values than Ni₃Al alloy values; this is related to the stability of a passive layer formed on the coating surface [37].

A similar behavior is observed in the case of NiAl coatings. Its corrosion potential tends to increase dramatically during the first 24 hours then remain nearly constant reaching more positive values than values of the base alloy. All coatings showed anodic behavior after the first day of immersion compared to the substrate.

3.4.3 Polarization resistance

Figures 13 and 14 show the variation of the corrosion current density of coatings, intermetallic alloys and 304 SS obtained from the measurements of polarization resistance in 1.0 M NaOH at 25 °C. The 304 stainless steel had the highest corrosion rate with a clear tendency to increase from the fourth day of trial. Ni₃Al intermetallic alloy was the material with the lowest corrosion rate with a very stable performance during the whole period test. NiAl intermetallic alloy also showed a lower corrosion rate than that of stainless steel but slightly greater than the corrosion of the Ni₃Al intermetallic alloy.

Ni₃Al coatings showed higher corrosion rates than intermetallic alloys but lower than that shown by 304 SS. Coarse and medium grain size coatings deposited by flame sprayed process 5P11 had lower corrosion rates than fine grain coatings. It is possible that the low performance of this coating is associated to the presence of oxides trapped during the spray process of the fine particles. Since it is known that the pre-oxidized particles deposited during the spray process can affect the corrosion performance of the coatings [26]. By contrast, only the coarse grain size, deposited by the HVOF process was the one with the smallest corrosion rate compared to coatings of medium and fine particle size. However, despite these differences, the corrosion rates are similar and they are in the same order of magnitude.

On the other hand, it was observed that NiAl coatings showed similar behavior to that of the Ni₃Al coatings. Their corrosion rates were lower than that of stainless steel, and in particular the coarse and medium particle size coatings showed lower corrosion rates than the NiAl intermetallic based alloy. In general materials with high aluminum content had lower corrosion rates in NaOH solutions. This is mainly due both the oxides and hydroxides of Al have protective properties. Since the OH⁻ ions react with the metallic surface and form precipitates of Al(OH)₃ with protective characteristics [26, 38-39].

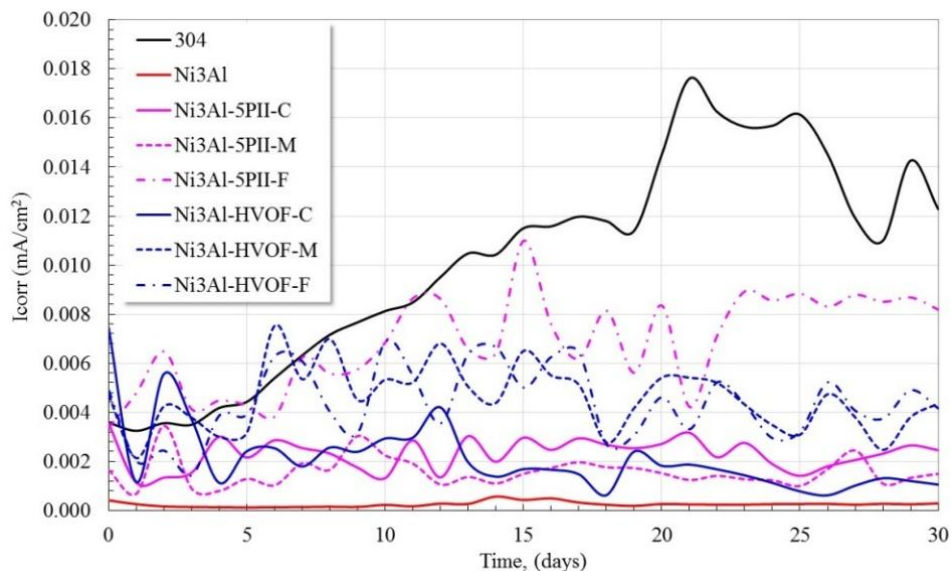


Figure 13. Corrosion current density of Ni₃Al coatings and alloys in 1.0 M NaOH at 25 °C.

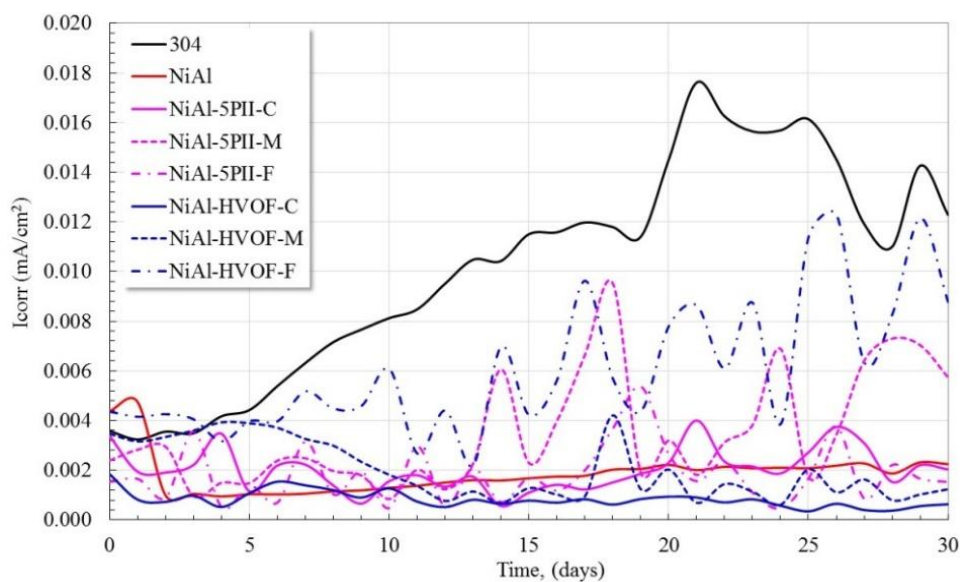


Figure 14. Corrosion current density of NiAl coatings and alloys in 1.0 M NaOH at 25 °C.

4. CONCLUSIONS

The microstructural characteristics of coatings depend strongly on the application process, application parameters and particle size. Major differences observed among coatings were the presence of semi-molten particles trapped between the oxide layers and porosity. Coatings applied by the HVOF process regardless of particle size showed greater resistance to corrosion than coatings applied by the process of oxy-acetylene flame. However, the effect of particle size between HVOF applied coatings had a marginal effect on the coatings corrosion resistance.

ACKNOWLEDGEMENTS

Financial support from Consejo Nacional de Ciencia y Tecnología (CONACYT, México) (Project 198687) is gratefully acknowledged.

Conflict of Interests

The authors declare that there is no conflict of interests regarding the publication of this paper.

References

1. N. Cinca, C.R.C. Lima, J.M. Guilemany, *J. Mater. Res. Technol.*, 2 (2013) 75-86.
2. G.D. Sulka, P. Józwiak, *Intermetallics*, 19 (2011) 974-981.
3. A. Albiter, M.A. Espinosa-Medina, M. Casales, J.G. Gonzalez-Rodriguez, *Journal of Applied Electrochemistry*, 34 (2004) 1141-1145.
4. E.F. Díaz, S. Sierra, J. Porcayo-Calderon, C. Cuevas, A. Torres-Islas, A. Molina, J. Colin, *Int. J. Electrochem Sci.*, 8 (2013) 7156-7174.
5. B. Szczucka-Lasota, B. Formanek, A. Hernas, K. Szymanski, *J. Mater. Process. Technol.*, 164–165 (2005) 935–939.
6. T.C. Totemeier, R.N. Wright, W.D. Swank, *Intermetallics*, 12 (2004) 1335–1344.
7. H. Singh, D. Puri, S. Prakash, *Metall. Mater. Trans. A*, 36 (2005) 1007-1015.
8. K.R. Luer, J.N. DuPont, A.R. Marder, *Corrosion*, 56 (2000) 189-198.
9. J.M. Guilemany, C.R.C. Lima, N. Cinca, J. R. Miguel, *Surf. Coat. Technol.*, 201 (2006) 2072–2079.
10. J.M. Guilemany, N. Cinca, S. Dosta, C.R.C. Lima, *Intermetallics*, 15 (2007) 1384-1394.
11. G. Ji, O. Elkedim, T. Grosdidier, *Surf. Coat. Technol.*, 190 (2005) 406– 416.
12. H. Singh, D. Puri, S. Prakash, *Surf. Coat. Technol.*, 192 (2005) 27– 38.
13. B.S. Sidhu, S. Prakash, *Surf. Coat. Technol.*, 201 (2006) 1643–1654
14. N. Masahashi, S. Watanabe, S. Hanada, *ISIJ International*, 41 (2001) 1010–1017.
15. J.R. Blackford, R.A. Buckley, H. Jones, C. M. Sellars, D.G. McCartney, A.J. Horlock, *J. Mat. Sci.*, 33 (1998) 4417-4421.
16. Y. Wang, W. Chen, *Surf. Coat. Technol.*, 183 (2004) 18–28.
17. B.S. Lasota, B. Formanek, A. Hernas, *J. Mater. Process. Technol.*, 164–165 (2005) 930–934.
18. Y. Wang, W. Chen, *J. Mater. Sci. Lett.*, 22 (2003) 845– 848.
19. A. Scrivani, S. Ianelli, A. Rossi, R. Groppetti, F. Casadei, G. Rizzi, *Wear*, 250 (2001) 107–113.
20. M.B. Beardsley, *Lawrence Livermore National Laboratory*, Report LLNL-JRNL-402708 April 4, 2008.
21. J.M. Guilemany, N. Cinca, S. Dosta, A.V. Benedetti, *Corros. Sci.*, 51 (2009) 171–180.
22. M.M. Verdian, K. Raeissi, M. Salehi, *Corros. Sci.*, 52 (2010) 1052–1059.
23. S. Frangini, A. Masci, *Surf. Coat. Technol.*, 184 (2004) 31–39.
24. D. Chidambaram, C.R. Clayton, M.R. Dorfman, *Surface & Coating Technology*, 176 (2004) 307-317.
25. D. Chidambaram, C.R. Clayton, M.R. Dorfman, *Surface & Coating Technology*, 192 (2005) 278-28.
26. J. Porcayo-Calderon, C.D. Arrieta-Gonzalez, A. Luna-Ramírez, V.M. Salinas-Bravo, C. Cuevas-Arteaga, A. Bedolla-Jacuiende, L. Martínez-Gómez, *Int. J. Electrochem. Sci.*, 8 (2013) 12205-12218.
27. M.M. Javadi, H. Edris, M. Salehi, *J. Mater. Sci. Technol.*, 27 (2011) 816-820.
28. W. Pilarczyk, R. Nowosielski, M. Jodkowski, K. Labisz, H. Krztoń, *Archives of Materials Science and Engineering*, 31 (2008) 29-32.

29. Lech Pawlowski, *The Science and Engineering of Thermal Spray Coatings*, John Wiley & Sons Ltd, (Second edition) 2008.
30. T.C. Totemeier, R.N. Wright, W.D. Swank, *Metallurgical and Materials Transactions*, 34A (2003) 2223-2231.
31. T.C. Totemeier, R.N. Wright, W.D. Swank. *Journal of Thermal Spray Technology*, 11(2002) 400-408.
32. I. Gedzevicius, A.V. Valiulis, *Materials Science (Medziagotyra)*, 9 (2003) 334-337.
33. A.P. Newbery, P.S. Grant, *Journal of Materials Processing Technology*, 178 (2006) 259-269.
34. M.M. Verdian, *Surface Engineering*, 27 (2011) 504-508.
35. E.A. Esfahani, H. Salimajazi, M.A. Golozar, J. Mostaghimi, L. Pershin, *Journal of Thermal Spray Technology*, 21 (2012) 1195-1202.
36. J.M. Guilemany, J. Fernandez, N. Espallargas, P.H. Suegama, A.V. Benedetti, *Surface & Coatings Technology*, 200 (2006) 3064-3072.
37. Y. Santana-Jimenez, M. Tejera-Gil, M. Torrado-Guerra, L.S. Baltes, J.C. Mirza-Rosca, *Bulletin of the Transilvania University of Braşov*, 2 (2009) 197-204.
38. S.S. Abd-El Rehim, S.S. Abd-El Haleem, S.M. Abd-El Wahaab and M. Sh. Shalaby, *Surf. Technol.*, 19 (1983) 261-271.
39. M.L. Doche, J.J. Rameau, R. Durand, F. Novel-Cattin, *Corros. Sci.*, 41(1999) 805-826.

© 2015 The Authors. Published by ESG (www.electrochemsci.org). This article is an open access article distributed under the terms and conditions of the Creative Commons Attribution license (<http://creativecommons.org/licenses/by/4.0/>).